PHYSICAL REVIEW B VOLUME 25, NUMBER 5 1 MARCH 1982

Surfaces and interfaces of lattice models: Mean-field theory as an area-preserving map

Rahul Pandit and Michael Wortis
Department of Physics and Materials Research Laboratory, University of Illinois at Urbana-Champaign, Urbana, Illinois 61801
(Received 13 October 1981)

Mean-field theory for one-dimensionally inhomogeneous magnetic systems is formulated as an area-preserving map. The map and its associated boundary conditions are derived for nearest-neighbor Ising interactions. The corresponding continuum theory is also constructed. These mappings are two dimensional. Their phase portraits are exhibited and applied to the study of a representative set of surface and interface phenomena, including interfacial structure, surface phase transitions, wetting, prewetting, and layering. The methods developed lend themselves to easy and physical visualization of the types of solutions which the mean-field theory can have, even in rather complex situations. They also make explicit the fundamental differences between continuum mean-field theory (which is integrable) and discrete mean-field theory (which is not).

I. INTRODUCTION

Many problems in condensed-matter physics involve the study of a d-dimensional sample with local average properties which vary along one space direction, but are homogeneous in the remaining $(d-1)$ orthogonal directions. Simple examples include both bulk properties of layered materials[1-3] and surface or interface properties of materials which in the bulk would be homogeneous. Such systems have been studied recently by a large variety of methods. Mean-field theory often (but not always[4]) provides a useful first approximation. It is the purpose of this paper to explore the observation that the mean-field theory of one-dimensionally inhomogeneous systems may be regarded as a problem in nonlinear dynamics[5] subject to appropriate boundary conditions. What makes this point of view useful is that the phase portrait of the appropriate nonlinear map exhibits in a particularly graphic way the kinds of solutions which the theory can have and, hence, the types of physical phenomena to be expected. The mean-field map turns out to be area-preserving. The generic features of its phase portraits depend crucially on whether or not the map is integrable.[6]

We consider for specificity the Ising model on a d-dimensional hypercubical lattice[7] and take the inhomogeneity to be along the x direction. If the local magnetization density $M(x)$ is regarded as continuous, then the (differential) mapping turns out to be integrable and the phase portraits are rather simple. On the other hand, when the layers are regarded as discrete, the mapping is nonintegrable and the phase portraits are more complex. In the former case mean-field theory allows only a finite (small) number of phase transitions; in the latter, there is the possibility of infinite sequences of distinct layer transitions.[8,9] This possibility is realized in some physical situations and not in others. When such sequences of "layer" transitions occur, the continuum theory cannot in any direct way be regarded as an approximation to the discrete theory.

Section II develops the nonlinear maps for both the continuum and discrete cases. Section III displays the important features of their phase portraits. Section IV applies the phase portraits developed in Sec. III to several typical surface and interface problems. The focus here is on developing appropriate boundary conditions to characterize the dynamical problem and explaining the differences between the integrable and nonintegrable versions of each problem. An appendix reviews additional interesting properties of the phase portraits which are not important in the examples discussed here but may play a role in other contexts.

We emphasize that actual mean-field solutions found by our methods are no different from those

found by any other methods. Our contribution, such as it is, is a different point of view, which lends itself to different insights. A final disclaimer: It is well known that mean-field predictions may or may not be fundamentally modified by proper inclusion of thermal fluctuations. We shall comment briefly on this point but detailed discussion is beyond the scope of this paper.

II. MEAN-FIELD THEORY AND NONLINEAR MAPS

The $s=\frac{1}{2}$ Ising model is defined by the Hamiltonian,

$$\mathcal{H}=-\sum_i H_i\sigma_i-\sum_{\langle ij\rangle} J_{ij}\sigma_i\sigma_j,\quad \sigma=\pm 1 \tag{1}$$

where subscripts label lattice sites and the sum $\langle ij\rangle$ is over distinct pairs. H_i is the magnetic field at site i and J_{ij} is the exchange coupling between sites i and j. The free energy of this model is (in units such that Boltzmann's constant $k_B=1$)

$$F=-T\ln \mathrm{Tr}\exp(-\mathcal{H}/T)\ ,$$

where T is the temperature. The thermal average magnetization of the ith spin is $M_i=\langle\sigma_i\rangle$. Within the context of mean-field theory F and $\{M_i\}$ may be found by minimizing the functional,[10]

$$\begin{aligned}\mathcal{F}[\{\mathcal{M}_i\};T,\{H_i\},\{J_{ij}\}]&=-\sum_i H_i\mathcal{M}_i+T\sum_i\int_0^{\mathcal{M}_i} dy\tanh^{-1}y\\&\quad-\sum_{\langle ij\rangle} J_{ij}\mathcal{M}_i\mathcal{M}_j\ ,\end{aligned} \tag{2}$$

with respect to the variational parameters $\{\mathcal{M}_i\}$. At the (global) minimum

$$(\mathcal{F})_{\min}=F[T,\{H_i\},\{J_{ij}\}]$$

and (3)

$$(\mathcal{M}_i)_{\min}=M_i[T,\{H_i\},\{J_{ij}\}]\ .$$

Suppose now that all quantities may vary in the x direction but remain translationally uniform in directions perpendicular to x. Denote by H_n and $\mathcal{M}_n$ the magnetic field acting on the nth-layer spins and the magnetization of a spin in the nth layer. Furthermore, define interlayer couplings

$$K_{mn}=\sum_{j\in n} J_{ij}=K_{nm}\ , \tag{4}$$

where i is any (specific) site in the mth layer and j is summed over all nth-layer sites. Under the assumption of one-dimensional inhomogeneity the variational function (2) takes the form,

$$\begin{aligned}L^{-(d-1)}\mathcal{F}[\{\mathcal{M}_n\};T,\{H_n\},\{K_{mn}\}]&=-\sum_n\left[H_n\mathcal{M}_n-T\int_0^{\mathcal{M}_n} dy\tanh^{-1}y\right]\\&\quad-\tfrac{1}{2}\sum_{m,n}K_{mn}\mathcal{M}_m\mathcal{M}_n\ ,\end{aligned} \tag{5}$$

where L^{d-1} is the number of sites per layer.[11] The condition $\partial\mathcal{F}/\partial\mathcal{M}_n=0$ that $\mathcal{F}$ be extremal leads to the usual mean-field equations,

$$H_n+\sum_m K_{nm}\mathcal{M}_m=T\tanh^{-1}\mathcal{M}_n\ . \tag{6}$$

Equation (6) will provide the nonlinear mapping which we shall study.

If the interactions J_{ij} are of finite range, then there is a maximum layer spacing Q beyond which layers do not interact directly, i.e., $K_{mn}=0$ for all $|n-m|>Q$. Then, Eq. (6) can be solved to obtain the magnetization $\mathcal{M}_{n+2Q+1}$ in terms of that of the preceding $2Q$ layers, $\mathcal{M}_{n+1}$, $\mathcal{M}_{n+2}$, . . . , $\mathcal{M}_{n+2Q}$. We can therefore define a $2Q$-dimensional map which translates layers $n+1,n+2,\ldots,n+2Q$ into layers $n+2,n+3,\ldots,n+2Q+1$,

$$\mathcal{M}'_{n+m}=\mathcal{M}_{n+m+1}\quad\text{for } m=1,\ldots,2Q-1 \tag{7a}$$

$$\mathcal{M}'_{n+2Q}=\mathcal{M}_{n+2Q+1}\ (\mathcal{M}_{n+1},\mathcal{M}_{n+2},\ldots,\mathcal{M}_{n+2Q})\ . \tag{7b}$$

The fields $\{H_n\}$ and interlayer couplings $\{K_{mn}\}$ enter only into Eq. (7b). When the interactions are translationally invariant in the x direction,

$$H_n=H\quad\text{for all } n\ , \tag{8a}$$

$$K_{mn}=K(n-m)=K(m-n)\ , \tag{8b}$$

and the mapping $\mathcal{M}_{n+2Q+1}\ (\mathcal{M}_{n+1},\mathcal{M}_{n+2},\ldots,\mathcal{M}_{2Q})$ in Eq. (7b) no longer depends explicitly on n. It is straightforward to compute the Jacobian of the map (7),

$$J(\mathcal{M}',\mathcal{M})=\frac{\partial\mathcal{M}'_{n+2Q}}{\partial\mathcal{M}_{n+1}}=\frac{K_{n+Q+1,n+1}}{K_{n+Q+1,n+2Q+1}}\ . \tag{9}$$

When the interactions are translationally invariant, Eq. (8b) holds, $J(\mathcal{M}',\mathcal{M})=1$, and the map (7) is area-preserving.

Different physical problems require different interactions $\{H_n\}$, $\{K_{mn}\}$. The so-called ANNNI

(axial next-nearest-neighbor Ising) model[1] is translationally uniform in the x direction [so Eq. (8) applies] and requires interactions between next-nearest-neighbor layers (so $Q=2$). The map (7) is then four dimensional. A two-dimensional approximation to this system was recently treated by Bak.[12] For the surface and interface problems which we shall use as examples in what follows, it suffices to consider nearest-neighbor interactions only. For the homogeneous system we shall take

$$J_{ij}=J \text{ for all nearest-neighbor pairs } i,j \ , \qquad H_i=H \text{ for all sites } i \ . \tag{10}$$

Thus, $Q=1$ and for the hypercubical lattice (which we shall consider henceforth),

$$K_{n,n}=2(d-1)J \ , \quad K_{n,n+1}=J \ , \quad H_n=H \ . \tag{11}$$

The free-energy functional (5) becomes

$$L^{-(d-1)}\mathcal{F}[\{\mathcal{M}_n\}]=\sum_{n=-\infty}^{\infty} g(\mathcal{M}_n,\mathcal{M}_{n+1}) \ ,$$

with

$$g(\mathcal{M}_n,\mathcal{M}_{n+1})\equiv \frac{J}{2}(\mathcal{M}_{n+1}-\mathcal{M}_n)^2 + T\int_0^{\mathcal{M}_n} dy \tanh^{-1}y - dJ\mathcal{M}_n^2 - H\mathcal{M}_n \ . \tag{12}$$

Differentiation $\partial\mathcal{F}/\partial\mathcal{M}_n=0$ leads to Eq. (6) in the form,

$$H+J(\mathcal{M}_{n+1}-2\mathcal{M}_n+\mathcal{M}_{n-1})+2dJ\mathcal{M}_n = T\tanh^{-1}\mathcal{M}_n \ , \tag{13}$$

and the map (7) is

$$\mathcal{M}'_{n+1}=f_1(\mathcal{M}_{n+1},\mathcal{M}_{n+2})=\mathcal{M}_{n+2} \ , \tag{14a}$$

$$\mathcal{M}'_{n+2}=f_2(\mathcal{M}_{n+1},\mathcal{M}_{n+2}) = \frac{T}{J}\tanh^{-1}\mathcal{M}_{n+2} - 2(d-1)\mathcal{M}_{n+2}-\mathcal{M}_{n+1}-\frac{H}{J} \ . \tag{14b}$$

The two-dimensional map f_1,f_2 is area-preserving and independent of n.

It is instructive to develop for comparison continuum analogs of Eqs. (12) and (13). Let the local magnetization $\mathcal{M}(x)$ now depend on a continuous variable x. The appropriate analogs are

$$L^{-(d-1)}\mathcal{F}[\mathcal{M}(x)]=\int_{-\infty}^{\infty} dx\, g\left[\mathcal{M}(x),\frac{d\mathcal{M}(x)}{dx}\right] \ ,$$

with

$$g\left[\mathcal{M}(x),\frac{d\mathcal{M}(x)}{dx}\right]=\frac{J}{2}\left[\frac{d\mathcal{M}(x)}{dx}\right]^2 + T\int_0^{\mathcal{M}(x)} dy \tanh^{-1}y - dJ\mathcal{M}^2(x)-H\mathcal{M}(x) \ , \tag{15}$$

and

$$H+J\frac{d^2\mathcal{M}(x)}{dx^2}+2dJ\mathcal{M}(x)=T\tanh^{-1}\mathcal{M}(x) \ , \tag{16}$$

which follows from Eq. (15) by the variation $\delta\mathcal{F}[\mathcal{M}]/\delta\mathcal{M}(x)=0$. When there is no spatial variation, Eqs. (15) and (16) are identical to Eqs. (12) and (13) at all T,H. When there is spatial variation, then Eq. (16) can approximate those solutions of Eq. (13) for which such variation is slow on the scale of the interlayer spacing. If this is so, then

$$\mathcal{M}_{n+1}-\mathcal{M}_n\approx\left.\frac{d\mathcal{M}(x)}{dx}\right|_{x=n} \ , \qquad \mathcal{M}_{n+1}-2\mathcal{M}_n+\mathcal{M}_{n-1}\approx\left.\frac{d^2\mathcal{M}(x)}{dx^2}\right|_{x=n} \ .$$

A necessary but not sufficient condition is[13] that the correlation length $\xi>>1$ (i.e., $H\approx 0$ and $T\approx T_c=2dJ$). Note that Eq. (16) can be written in a two-dimensional form directly analogous[14] to Eq. (14),

$$\frac{d\mathcal{M}(x)}{dx}=g_1(\mathcal{M}(x),\dot{\mathcal{M}}(x))=\dot{\mathcal{M}}(x) \ , \qquad \frac{d\dot{\mathcal{M}}(x)}{dx}=g_2(\mathcal{M}(x),\dot{\mathcal{M}}(x)) = \frac{T}{J}\tanh^{-1}\mathcal{M}(x)-2d\mathcal{M}(x)-\frac{H}{J} \ . \tag{17}$$

The condition that such a map be area-preserving is

$$\frac{\partial g_1}{\partial \mathcal{M}}+\frac{\partial g_2}{\partial \mathcal{M}}=0 ,$$

which is trivially satisifed by Eq. (17).

We wish finally to introduce a free surface into the theory. It will be useful to have the possibility of modifying the magnetic field and exchange coupling in the surface layer. Hence, we take $\mathcal{M}_n=0$ for all $n<1$ and

$$\begin{aligned} &J_{ij}=J(1+D) \text{ for } i,j \text{ in layer } n=1 , \\ &H_i=H+h_1 \text{ for } i \text{ in layer } n=1 . \end{aligned} \tag{18}$$

D is called the surface enhancement.[15] h_1 is the surface layer field.[15] This modifies Eq. (11) to

$$\begin{aligned} &K_{1,1}=2(d-1)(1+D)J , \\ &H_1=H+h_1 . \end{aligned} \tag{19}$$

The free-energy functional (12) becomes

$$L^{-(d-1)}\mathcal{F}[\{\mathcal{M}_n\}]=\sum_{n=1}^{\infty} g(\mathcal{M}_n,\mathcal{M}_{n+1}) + \frac{J}{2}[1-2(d-1)D]\mathcal{M}_1^2-h_1\mathcal{M}_1 , \tag{20}$$

which leads to a modification of Eq. (13) for the surface layer $n=1$,

$$H+h_1+J(\mathcal{M}_2-\mathcal{M}_1)+2dJ\mathcal{M}_1 -J\mathcal{M}_1[1-2(d-1)D]=T\tanh^{-1}\mathcal{M}_1 . \tag{21}$$

Notice, by comparing with the uniform equation (13), that the boundary condition (21) is completely equivalent to the introduction of a fictitious $n=0$ layer with

$$\mathcal{M}_0=h_1/J+2(d-1)D\mathcal{M}_1 . \tag{22}$$

The corresponding modification of the continuum theory[16] takes the form

$$L^{-(d-1)}\mathcal{F}[\mathcal{M}(x)]=\int_0^{\infty} dx\, g\left[\mathcal{M}(x),\frac{d\mathcal{M}(x)}{dx}\right] + \frac{J}{2}[1-2(d-1)D]\mathcal{M}^2(0) -h_1\mathcal{M}(0) . \tag{23}$$

Variation with respect to $\mathcal{M}(0)$ leads to the boundary condition,[17]

$$J\frac{d\mathcal{M}(x)}{dx}\bigg|_{x=0}+h_1-J\mathcal{M}(0)[1-2(d-1)D]=0 , \tag{24}$$

which is analogous to Eq. (21). We emphasize, however, that the introduction of a surface always involves inhomogeneity, so Eq. (24) can only be an approximation to Eq. (21) when $\xi>>1$ and, even then, requires that the surface perturbations be sufficiently weak so that they do not lead to strong inhomogeneity. To make this concrete, notice that adding Eq. (21) to the sum of Eq. (13) over layers $m=2,\ldots,n$ produces the discrete analog of Eq. (24),

$$J(\mathcal{M}_{n+1}-\mathcal{M}_n)+h_1-J\mathcal{M}_1[1-2(d-1)D] =\sum_{m=1}^{n}(T\tanh^{-1}\mathcal{M}_m-2dJ\mathcal{M}_m-H) . \tag{25}$$

For $1<<n<<\xi$, the left side of Eq. (25) agrees with Eq. (24); however, the right-hand side is not small unless the surface perturbation is weak.

III. PHASE PORTRAITS

In this section we describe the fixed points of the area-preserving maps (14) and (17) and their associated trajectories, since it is these features that we shall need for the physical examples to be discussed in Sec. IV. The Appendix contains a brief discussion of additional properties of these maps.

The fixed points of both Eqs. (14) and (17) correspond to a spatially uniform magnetization distribution given by solutions of the usual mean-field equation of state,

$$H+2dJ\mathcal{M}=T\tanh^{-1}\mathcal{M} . \tag{26}$$

Equation (26) has either one or three solutions depending on T,H, as shown[18] in Fig. 1. Of course, only that one of the three solutions which minimizes the free-energy functional (12) or (15) is thermodynamically stable for a homogeneous bulk system. In the presence of surface or interface inhomogeneity, other fixed points can play a role, as we shall see in Sec. IV. Local structure near the fixed points is qualitatively the same in the continuous and discrete cases; however, global behavior of the insets (inflowing orbits) and outsets (outflowing orbits) of the hyperbolic fixed points is entirely different.

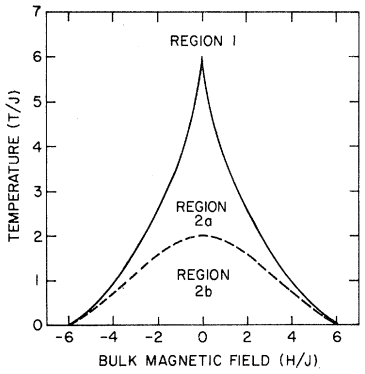

FIG. 1. Different regimes for uniform mean-field theory ($d=3$). In region 1 the mean-field equation (26) has a unique solution, corresponding to a single hyperbolic fixed point P_0 of Eqs. (14) or (17). In region 2, there are three solutions corresponding to the fixed points $P_\pm$ (hyperbolic) and P_0. In the continuum theory P_0 is always elliptic. In the discrete theory P_0 is elliptic in region 2a but becomes hyperbolic with reflection in region 2b.

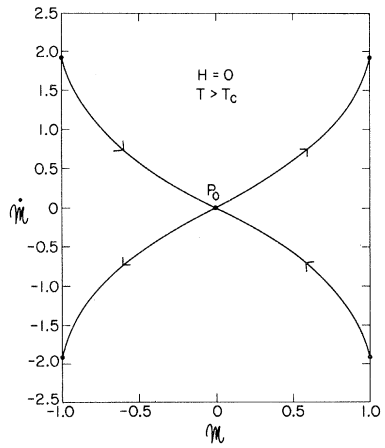

FIG. 2. Phase portrait for the continuum theory Eq. (17) in region 1 (Fig. 1), showing the unique thermodynamically stable fixed point P_0 along with its insets and outsets. Data for this plot are $d=3$, $H=0$, $T=7J$. Nonzero H would shift P_0 away from $\mathcal{M}=0$. Note that the graph is restricted to $|\mathcal{M}| \leq 1$ and that the insets and outsets intersect $|\mathcal{M}|=1$ at finite values of $\mathcal{M}$.

A. Continuous case

Multiplication by $d\mathcal{M}(x)/dx$ makes Eq. (16) readily integrable and leads to a constant of the motion,

$$E=\frac{J}{2}\left[\frac{d\mathcal{M}(x)}{dx}\right]^2-T\int_0^{\mathcal{M}(x)}dy\,\tanh^{-1}y$$

$$+dJ\mathcal{M}^2(x)+H\mathcal{M}(x)\,. \tag{27}$$

When E is set to its fixed-point value, Eq. (26) can be solved for the insets and outsets. These sets are shown in Figs. 2, 4, and 6 for representative cases. For real $\mathcal{M}$ the function $\tanh^{-1}\mathcal{M}$ exists only for $|\mathcal{M}|<1$, so the figures are restricted to this interval. Because Eq. (17) is area-preserving, the characteristic fixed-point (FP) eigenvalues σ_1, σ_2 of the 2×2 matrix $\partial g/\partial(\mathcal{M},\dot{\mathcal{M}})\,|_{\rm FP}$ sum to zero. In fact,

$$\sigma_i^2=\frac{T}{J}\left[\frac{1}{1-\mathcal{M}^2}\right]-2d\,. \tag{28}$$

In region 1 of Fig. 1 there is a single thermodynamically stable hyperbolic ($\sigma_i^2>0$) fixed point P_0 (see Fig. 2), with nonintersecting insets and outsets. In region 2 of Fig. 1 there are three fixed points. The central one, (P_0), is elliptic ($\sigma_i^2<0$) and has no inflowing or outflowing orbits. The outer ones (P_+ and P_-) are hyperbolic. When $H=0$ (Fig. 4), both P_+ and P_- are thermodynamically stable (corresponding to "up" and "down" stable phases at coexistence) and are joined by two (heteroclinic) trajectories. For $H<0$ (Fig. 6) only P_- is thermodynamically stable, while P_+

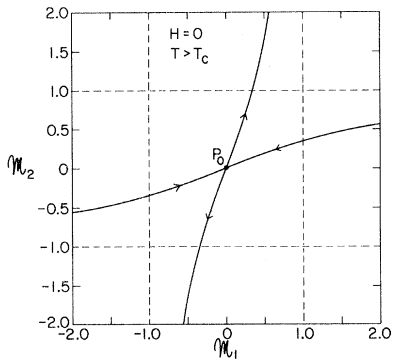

FIG. 3. Phase portrait for the discrete theory Eq. (14) in region 1 (Fig. 1), showing the unique thermodynamically stable fixed point P_0 with its insets and outsets. Data are the same as for Fig. 2. The different variables used in the discrete theory have the effect of rotating Fig. 3 relative to Fig. 2 by $\pi/4$. Note that insets must have $|\mathcal{M}_2|<1$, while outsets must have $|\mathcal{M}_1|<1$.

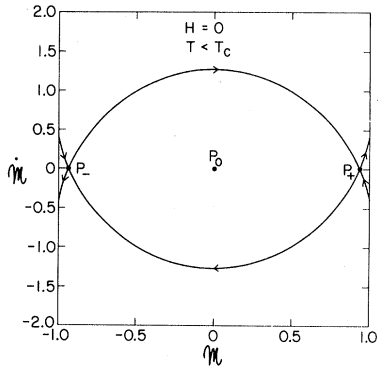

FIG. 4. Phase portrait for the continuum theory Eq. (17) in region 2 of Fig. 1 for $H=0$, showing the three points, P_0, P_+, and P_-, and the insets and outsets. Data for this figure are $d=3$, $T=3.3J$. At $H=0$ both P_+ and P_- are thermodynamically stable but P_0 is unstable. P_0 is elliptic and has no inset or outset.

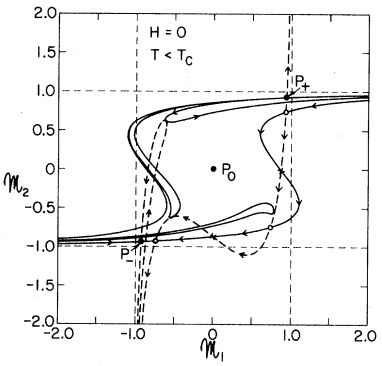

FIG. 5. Phase portrait for the discrete theory Eq. (14) in region 2a of Fig. 1 for $H=0$. The three fixed points, P_0, P_+, and P_- are shown. P_+ and P_- are thermodynamically stable; P_0 is unstable. Data are the same as for Fig. 4. The nonintegrability of Eq. (14) leads to insets and outsets of P_+ and P_- that do not terminate, as do their counterparts in the continuum theory Eq. (17), but continue indefinitely. For simplicity only a part of the inset of P_- (solid line) and a part of the outset of P_+ (dashed line) are shown. The corresponding parts of the outset of P_- and the inset of P_+ may be constructed by symmetry (see text). The circles and crosses mark members of two different trajectories of heteroclinic points which join P_+ to P_- and represent possible mean-field interfacial profiles (Sec. IV A). Additional circles and crosses which should mark the remainder of these trajectories are not shown because they get crowded below P_+ and to the right of P_-, where the inset of P_+ and the outset of P_- cross each other an infinite number of times on a finer and finer scale. The circle trajectory has lower free energy and describes the equilibrium interface.

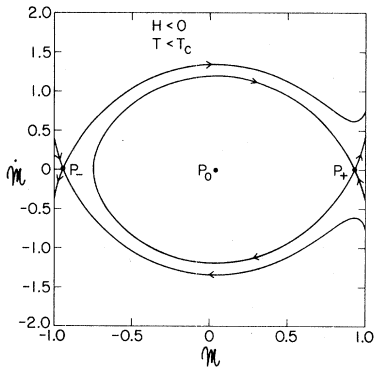

FIG. 6. Phase portrait for the continuum theory Eq. (17) in region 2 of Fig. 1 for $H<0$, showing the three fixed points, P_0, P_+, and P_-, and their insets and outsets. Data for this figure are $d=3$, $H/J=-0.1$, $T/J=3.3$. For $H<0$ only P_- is thermodynamically stable. Note that P_+ has developed a homoclinic orbit. When $|H|$ is small, the inset of P_- passes close to P_+.

develops a homoclinic orbit. As $|H|$ is increased to the boundary between regions 1 and 2 (Fig. 1), P_0 and P_+ come together and annihilate.[19] Similar statements obtain for $H>0$ with the roles of P_+ and P_- interchanged.

B. Discrete case

We study the discrete map[20] in the form[14] (14). This has the effect of rotating the phase portraits by $\pi/4$ relative to the continuous case, so the fixed points lie on the diagonal $\mathcal{M}_1=\mathcal{M}_2$. This map is not integrable. The phase portraits were computed numerically[21] and are shown as Figs. 3, 5, and 7. The map is discrete, so the orbits are not simply limited to the region $|\mathcal{M}|<1$: Eq. (14b) requires only that inset points have $|\mathcal{M}_2|<1$, while (14a) requires that outset points have $|\mathcal{M}_1|<1$. Indeed, the image under Eq. (14) of the line $\mathcal{M}_2=1^-$ [$\mathcal{M}_2=-1^+$] is the point $(\mathcal{M}'_1,\mathcal{M}'_2)=(1^-,\infty)$ [$(-1^+,-\infty)$], while the preimage under Eq. (14) of the line $\mathcal{M}'_1=1^-$ [$\mathcal{M}'_1=-1^+$] is the point $(\mathcal{M}_1,\mathcal{M}_2)=(\infty,1^-)$ [$(-\infty,-1^+)$]. We note finally that the area-preserving property requires that the fixed-point eigenvalues Λ_1, Λ_2 of the 2×2 Jacobian matrix $\partial(\mathcal{M}'_1,\mathcal{M}'_2)/\partial(\mathcal{M}_1,\mathcal{M}_2)$ satisfy $\Lambda_1=\Lambda_2^{-1}$.

In region 1 of Fig. 1 the fixed point P_0 is hyperbolic (Λ_i real, positive, $\neq1$) and its insets and outsets are qualitatively similar to those of Fig. 2. P_0 is thermodynamically unstable[19] throughout region 2. It is elliptic ($\Lambda_1=\Lambda_2^*\neq1$) in region 2a but

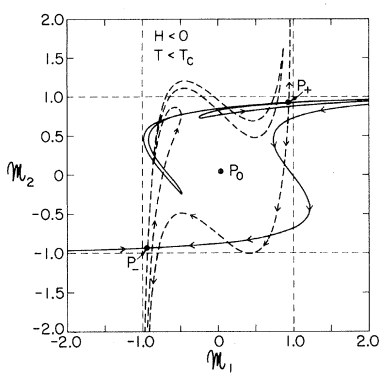

FIG. 7. Phase portrait for the discrete theory Eq. (14) in region 2a of Fig. 1 for $H<0$. The three fixed points P_0, P_+, and P_- are shown. P_- is thermodynamically stable; P_0 and P_+ are unstable. Data are the same as for Fig. 6. For simplicity only a part of the inset of P_- (solid line) and a part of the outset of P_+ (dashed line) are shown. The corresponding parts of the outset of P_- and the inset of P_+ may be constructed by symmetry (see text).

becomes hyperbolic with reflection (Λ_i real, negative, $\neq -1$) in region 2b. P_+ and P_- are hyperbolic throughout region 2. For $H=0$, P_+ and P_- are thermodynamically stable; however, they are not (cf., the continuous case) joined by a heteroclinic orbit. Instead, as shown[22] in Fig. 5, the inset of P_- intersects the outset of P_+. These intersections are called heteroclinic points and will play a role in the discussion of the interface problem in Sec. IV. Because the insets and outsets are invariant under the map (14), the existence of a single heteroclinic point implies the existence of an infinite number of them. Also, the inset of P_+ (P_-) intersects the outset of P_+ (P_-) at an infinite number of points called homoclinic points. The insets and outsets do not terminate (as in the continuum case) but continue indefinitely, creating a "stringy" region on a finer and finer scale. The whole rather complicated structure is referred to as a "horseshoe" in the mathematical literature.[23] For the sake of simplicity we have shown[22] in Fig. 5 only a part of the inset of P_- and a part of the outset of P_+. The corresponding parts of the outset of P_- and the inset of P_+ may be constructed from these data by noting that the whole figure must have two symmetries: It goes into itself under $(\mathcal{M}_1,\mathcal{M}_2)\leftrightarrow(-\mathcal{M}_1,-\mathcal{M}_2)$, while under $(\mathcal{M}_1,\mathcal{M}_2)\leftrightarrow(\mathcal{M}_2,\mathcal{M}_1)$ outsets interchange with insets.[24] The whole structure is much richer than that of Fig. 4. Analogous structure appears for $H\neq 0$ in region 2, as shown in Fig. 7. For $H<0$, P_- is the thermodynamically stable fixed point. The homoclinic orbit of Fig. 6 no longer exists; however, there are an infinite number of homoclinic points in the vicinity of P_+. The inset of P_- intersects the outset of P_+ in an infinite number of heteroclinic points. In Fig. 7 we show a part of the inset of P_- and a part of the outset of P_+; the corresponding parts of the outset of P_- and the inset of P_+ may be obtained by noting that under $(\mathcal{M}_1,\mathcal{M}_2)\leftrightarrow(\mathcal{M}_2,\mathcal{M}_1)$ outsets interchange with insets. As $|H|$ is increased to the boundary between regions 1 and 2 (Fig. 1), P_0 and P_+ come together and annihilate, there are no longer any heteroclinic or homoclinic trajectories, and a phase portrait like Fig. 3, with P_0 shifted away from the origin, is obtained. For $H>0$ the behavior of the phase portraits is similar, with the roles of P_+ and P_- interchanged.

IV. APPLICATIONS

The trajectories described in Sec. III are useful in solving a variety of surface and interface problems in the mean-field approximation. In each case the phase-portrait approach identifies the solutions of the mean-field equations (6) subject to appropriate boundary conditions. When multiple solutions exist, then the original variational principle (3) requires that the solution with the lowest value of the free-energy functional $\mathcal{F}$ be chosen. This physical solution in general changes continuously as external parameters are varied; however, when (and if) the minimum free energy switches from one solution to another, then there is a phase transition.

A. Interfacial profile

Here we deal with a system having translationally invariant interactions $-\infty<n,x<\infty$ and containing two coexisting phases, so $H=0$ and $T<T_c=2dJ$. We take the "down" phase at $n,x\rightarrow+\infty$ and the "up" phase at $n,x\rightarrow-\infty$, so the appropriate boundary conditions are

$$\mathcal{M}(x)\rightarrow\mp\mathcal{M} \quad \text{as } x\rightarrow\pm\infty \tag{29a}$$

or

$$\mathcal{M}_n\rightarrow\mp\mathcal{M} \quad \text{as } n\rightarrow\pm\infty\ , \tag{29b}$$

where $\mathcal{M}$ is the magnitude of the fixed-point magnetization at $P_\pm$. Thus, the appropriate solutions

of the mean-field equations (14) or (17) are those which lie simultaneously on the inset of P_- and on the outset of P_+.

In the continuum case (Fig. 4), there is a single heteroclinic orbit joining P_+ to P_-, which determines the interfacial profile $M(x)$ uniquely (up to an overall translation).[25] In the corresponding discrete case (Fig. 5), the inset of P_- does not coincide with the outset of P_+. The solutions of Eq. (14) subject to Eq. (29a) are restricted to the set of heteroclinic points, where the outset of P_+ intersects the inset of P_-. In contrast to the continuous case there are now many (indeed, an infinite number of) discrete orbits connecting P_+ to P_-. Two of these orbits (some points of which are indicated on Fig. 5) go directly from P_+ to P_- and correspond, respectively, to an interface which is symmetric about a layer (crosses) (e.g., $\mathcal{M}_n + \mathcal{M}_{-n} = 0$) and to an interface which is symmetric about an interlayer (circles) (e.g., $\mathcal{M}_n + \mathcal{M}_{-n+1} = 0$). All others involve additional kink-antikink excitations, i.e., they start near P_+, spend time near P_-, return to the neighborhood of P_+, and then go to P_-, etc.[26] It is clear from Eq. (12) that these additional excitations cost extra free energy and will not appear at equilibrium. Of the two direct orbits, the interlayer-symmetric one has lower free energy for all $T < T_c$ and gives the equilibrium interacial profile $\{M_n\}$.

B. Surface enhancement and the surface transition

Here we consider the semi-infinite system,[15] Eqs. (18) and (19), with $H = h_1 = 0$ but $D \geq 0$. Boundary conditions deep in the material are

$$\mathcal{M}(x) \rightarrow \pm \mathcal{M} \ , \tag{29c}$$

as $x \rightarrow \infty$, and

$$\mathcal{M}_n \rightarrow \pm \mathcal{M} \ , \tag{29d}$$

as $n \rightarrow \infty$, while at the surface Eqs. (24) and (22) reduce, respectively, to,

$$\dot{\mathcal{M}}(0) = \mathcal{M}(0)[1 - 2(d-1)D] \ , \tag{30a}$$

and

$$\mathcal{M}_0 = 2(d-1)D\mathcal{M}_1 \ . \tag{30b}$$

Consider first the continuum case. The boundary conditions pick out the intersection of the inset of the appropriate bulk fixed point with the straight line (30a). For $T > T_c$, $\mathcal{M}(x) = 0$ is always a solution; however, two additional solutions appear when the initial inset slope at P_0 exceeds the slope of Eq. (30a), i.e., whenever

$$2(d-1)D - 1 > t^{1/2} \quad \text{with } t \equiv (T - T_c)/J \ . \tag{31}$$

When they exist, these solutions have lower free energy than $\mathcal{M}(x) = 0$ and correspond to the existence of a phase with spontaneous surface magnetization but no bulk magnetization.[15,27] Such a "surface ferromagnetic phase" occurs when the left side of Eq. (31) is positive,

$$D > D_c = \frac{1}{2(d-1)} \ . \tag{32}$$

This phase first appears via a second-order surface phase transition at the temperature $T_s(D)$ which makes Eq. (31) an equality. For $T < T_c$ (Fig. 4), $P_\pm$ become the appropriate fixed points and the intersection of their insets with Eq. (30a) is always unique, so no new phase transitions occur.

The discussion is similar for the discrete system. Written in terms of the map (14), $\mathcal{M}_i'(\mathcal{M}_1, \mathcal{M}_2)$, $i = 1,2$, the boundary condition (30b) reads (with appropriate relabeling of layers)

$$\mathcal{M}_2 = \mathcal{M}_1 / 2(d-1)D \ . \tag{33}$$

It is the intersection of Eq. (33) with the appropriate inset which determines the solutions of the mean-field equations plus boundary conditions. For $T > T_c$, $\mathcal{M}_n = 0$ is always a solution; however, two additional surface-phase solutions (with lower free energy) appear when

$$2(d-1)D - 1 > t/2 + [t + (t/2)^2]^{1/2} \ , \tag{34}$$

which agrees with Eq. (31) for $T \geq T_c$ and leads to Eq. (32). For $T < T_c$ there are (as for the interface) many solutions to mean-field theory. Those corresponding to down magnetization in the bulk may be visualized by superimposing the boundary condition (33) on Fig. 5. The lowest free energy is always attained for $\mathcal{M}_1 < 0$ and for the trajectory which flows directly to P_-.

There is every reason to believe that these phenomena persist beyond mean-field theory,[28] although with a value of D_c appropriately renormalized by thermal fluctuations.

C. Wetting, prewetting, and layering

We are again in the semi-infinite geometry but now take[29] $D = 0$, $H < 0$, and $h_1 > 0$, so the layer field h_1 biases the surface spins up, while the uniform field $H < 0$ forces the bulk magnetization

down. The boundary condition in the bulk is

$$\mathcal{M}(x)\to-\mathcal{M} \quad \text{as } x\to\infty \ , \tag{35a}$$

$$\mathcal{M}_n\to-\mathcal{M} \quad \text{as } n\to\infty \ , \tag{35b}$$

while Eqs. (24) and (22) become, respectively,

$$\dot{\mathcal{M}}(0)=\mathcal{M}(0)-h_1/J \tag{36a}$$

and

$$\mathcal{M}_0=h_1/J \ . \tag{36b}$$

Consider the continuum case first. For $T>T_c$ (Fig. 2), the straight line (36a) has a single intersection with the inset of P_0, indicating an excess surface magnetization induced by the layer field h_1, as expected. What happens for $T<T_c$ depends crucially on the magnitude of h_1/J.

1. *Critical wetting* $0<h_1/J<\alpha_1$

For small h_1 the situation is as pictured in Fig. 8(a). For $H<0$ the relevant inset of P_- starts at S and crosses the line LL' representing the boundary condition (36a) exactly once. The position of the intersection changes smoothly with T, so there is no phase transition at $H\neq 0$. Behavior in the limit $H\to 0-$ is, however, very sensitive to the value of T, because the inset then passes arbitrarily close to the fixed point P_+. When $T\approx T_c$ the distance between P_- and P_+ is small and the intersection occurs between S and P_+. Since flow past P_+ becomes slow as $H\to 0-$, this produces an arbitrarily thick region of "up" magnetization at the surface of the "down" bulk. This corresponds to the formation of a "wetting layer"[30] in the lattice-gas language.[29] The thickness of the wetting layer[16] diverges as $H\to 0-$ as $|\ln|H||$. As T decreases, the distance between P_+ and P_- grows and, for sufficiently low T, the line LL' intersects the inset of P_- between P_+ and P_-, so the thickness of the surface region of "up" magnetization is finite at $H=0^-$. The "critical wetting temperature," $T_W^{(c)}(h_1)$, which separates the two regimes, occurs when LL' passes through P_+, i.e., for

$$\mathcal{M}(T_W^{(c)},H=0)=h_1/J \ . \tag{37}$$

At $H=0^-$ the "up" surface region grows continuously to infinite thickness as T approaches $T_W^{(c)}$ from below. In this sense the transition is second order.[31] The limit of critical wetting is reached when the slope of the outset of P_+ at the intersection with LL' reaches unity, i.e., when

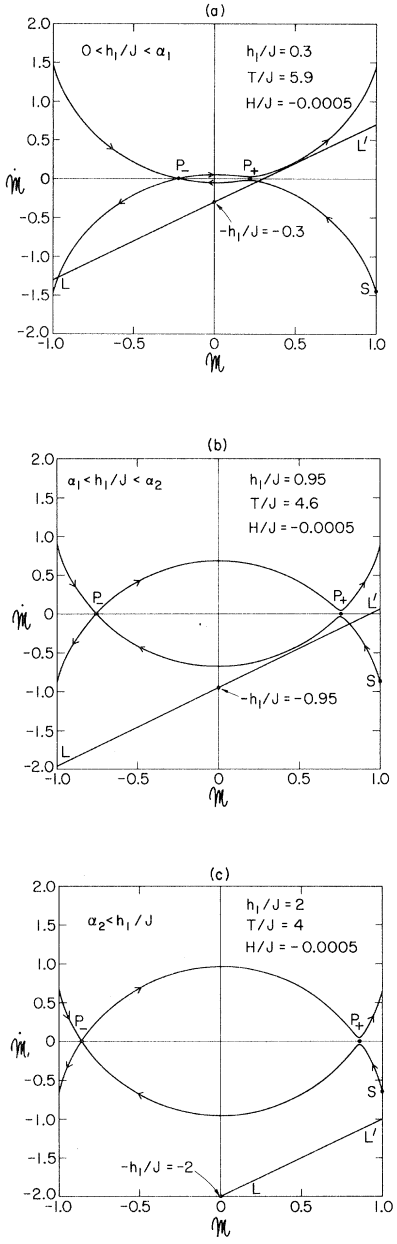

FIG. 8. Continuum phase portraits for $T<T_c$, $H\leq 0$, illustrating the mechanisms for critical wetting, first-order wetting, and layering. The straight line LL' must intersect the inset of the stable fixed point P_- for the boundary condition (36a) to be satisfied. (a) $0<h_1/J=0.3<\alpha_1$, $T=5.9J$, $H=-0.0005J$. (b) $\alpha_1<h_1/J=0.95<\alpha_2$, $T=4.6J$, $H=-0.0005J$. (c) $\alpha_2<h_1/J=2$, $T=4J$, $H=-0.0005J$.

$$\frac{T}{J}\frac{1}{1-\mathcal{M}^2}-2d=1 \ , \tag{38}$$

which gives (for $d=3$) $\alpha_1=0.453$ ($T_W^{(c)}=0.927T_c$).

2. *First-order wetting and prewetting,* $\alpha_1 < h_1/J < \alpha_2$

For $h_1/J \gtrsim \alpha_1$, the situation is as sketched in Fig. 8(b). At sufficiently high temperature LL' intersects the inset of P_- between S and P_+, so there is wetting as $H \to 0-$; however, now, as T decreases for $H = 0^-$, LL' becomes tangent to the inset of P_-. At a temperature $T_W^{(f)}$ slightly below the temperature at which tangency occurs ($T_W^{(f)}$ can be determined by an equal-area construction as shown in Fig. 4 of Ref. 16), the minimum-free-energy solution switches discontinuously from the segment SP_+ to the segment P_+P_-; thus, as T approaches $T_W^{(f)}$ from below, the thickness of the "up" surface region jumps discontinuously from some finite value to infinity at a first-order phase transition. This first-order behavior extends to nonzero H and terminates at a "prewetting critical point," as shown in Fig. 9. Wetting and prewetting have been discussed previously by Saam and Ebner,[32] Cahn,[16] Ebner,[33] Sullivan,[31] and others.[34] At sufficiently large h_1 the behavior changes again, as shown in Fig. 9. The mechanism, illustrated in Fig. 8(c), is the development of a range of T and H (shown shaded in Fig. 9) for which LL' does not

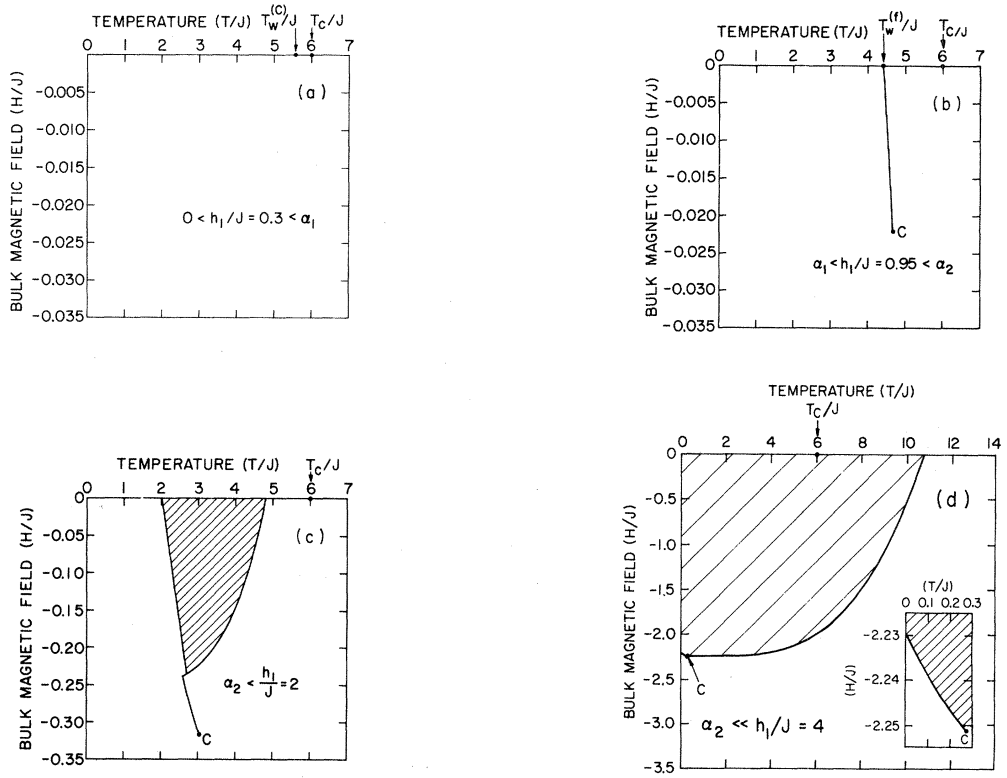

FIG. 9. Surface phase diagrams for the continuum description of wetting, prewetting, and layering. The point C is a critical point. The first-order line which attaches to C represents a discontinuity in the excess surface magnetization (or the excess surface density in the lattice-gas language). The shaded regions show where the boundary condition (36a) cannot be satisfied. (a) For weak layer field h_1 ($0 < h_1/J < \alpha_1$) there is no phase transition at $H < 0$ and $T_W^{(c)}(h_1)$ marks a continuous transition between an infinite "wetting" layer ($T > T_W^{(c)}$) and one of finite thickness ($T < T_W^{(c)}$). Data for this figure are $d = 3$, $h_1/J = 0.3$, $T_W^{(c)} = 5.815J$. (b) As h_1 increases ($\alpha_1 < h_1/J < \alpha_2$), prewetting develops and the transition at $T_W^{(f)}$ becomes first order. Data for this figure are $d = 3$, $h_1/J = 0.95$, $T_W^{(f)} = 4.41J$. (c) For $\alpha_2 \lesssim h_1/J$, a region (shown shaded) develops where the boundary condition cannot be satisfied (see text). Data for this figure are $d = 3$, $h_1/J = 2$. (d) For large h_1 ($\alpha_2 << h_1/J$), the region where the boundary condition cannot be satisifed becomes larger and larger and the first-order line gets pushed nearer and nearer the $T = 0$ axis. Data for this figure are $d = 3$, $h_1/J = 4$. The critical point C, the first-order line it is attached to, and the boundary of the shaded region near the $T = 0$ axis are shown on an expanded scale in the inset. The "elbow" which appears in the first-order phase boundary in (c) [also, in (d) but not visible on the scale shown] arises from a small region of parameters where the minimum-free-energy solution switches from the point S to the segment P_+P_- (Fig. 8). See also Ref. 35.

intersect the inset of P_-, so the boundary condition (36a) cannot be satisifed.[35] This first appears at $h_1/J=\alpha_2$, where (for $d=3$), $\alpha_2=1.46$ ($T_W^{(f)}=0.56T_c$).

3. *Layering, $h_1/J>\alpha_2$*

As h_1/J is increased beyond α_2, the region for which the boundary condition (36a) cannot be satisfied[35] continues to grow. The prewetting critical point and its associated first-order line move away from the T axis (see Fig. 9) and become a thin-layer-to-thick-layer transition, as H increases at fixed (low) T.

The discrete case is actually somewhat simpler. The boundary conditions (35b) and (36b) require that the inset of the appropriate bulk fixed point (see Figs. 3, 5, and 7) intersect the vertical line

$$\mathcal{M}_1=h_1/J\ . \tag{39}$$

This intersection is unique for $T>T_c$; however, for $T<T_c$ there are always an infinite number of solutions because of the "horseshoe" structure of the inset, described in Sec. III. These multiple solutions correspond, roughly speaking, to different numbers of "up" surface layers on top of the "down" bulk plus additional kink-antikink excitations. Kink-antikink excitations are expensive in free energy and do not occur at equilibrium. The new feature here, not present for the interface or the surface phase (Secs. IV A and IV B), is that the free-energy minimum switches from one intersection to another as a function of T and H, giving rise to an infinite sequence of first-order layer transitions,[8,33,36] as shown in Fig. 10. For $0<h_1/J<1$ and $H=0^-$ these transitions accumulate from below at a wetting temperature $T_W(h_1)$, while their associated critical points approach $T=T_c$, $H=0$. As $h_1/J\to 1-$, $T_W\to 0$. For $h_1/J>1$, the infinite sequence of layer transitions first noted by de Oliveira and Griffiths[8] is present.[36] We discuss in a separate publication[37] the details of this behavior and the extent to which it is modified by thermal fluctuations,[38] non-first-layer-only fields, etc.

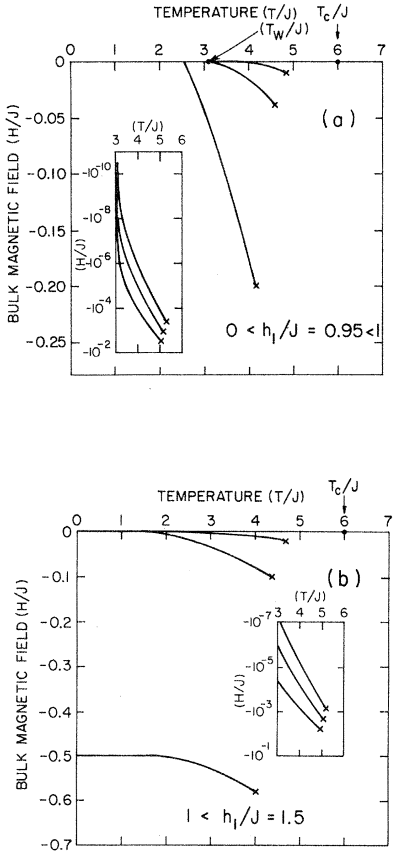

FIG. 10 Surface phase diagrams for the discrete description of wetting, prewetting, and layering. Because of the nonintegrability of Eq. (14), there are now an infinite number of distinct first-order layer transitions, each ending in a critical point (x). Within mean-field theory the critical points approach T_c (but see Ref. 38). (a) $0<h_1/J<1$, the first-order lines terminate at the T axis and accumulate at a wetting temperature $0<T_W<T_c$. When $h_1/J=1$, $T_W=0$. Data for the figure are $d=3$, $h_1/J=0.95$. T_W lies between $3.11J$ and $3.12J$. Only the first three first-order lines are shown completely. The inset shows the fourth, fifth, and sixth first-order lines on a semilogarithmic plot. (b) For $1<h_1/J$ all the first-order lines terminate at $T=H=0$, except for one which splits off and terminates on the negative H axis at $H=1-h_1/J$. Data for the figure are $d=3$, $h_1/J=1.5$. Only the first three first-order lines are shown completely. Parts of the fourth, fifth, and sixth first-order lines are shown on a semilogarithmic plot in the inset.

ACKNOWLEDGMENTS

We are grateful for useful advice and encouragement to E. Fradkin, C. Rottman, R. B. Griffiths, H. Nakanishi, M. Schick, and J. Wright. This work was supported in part by the National Science Foundation under Grants No. DMR 77-23999 and DMR 78-21069.

APPENDIX

In the main body of this paper we have concentrated on certain fixed points and their insets and outsets for the maps defined by Eqs. (14) and (17). In this appendix we give a brief description of the rest of the phase portraits of Eqs. (14) and (17). We shall only consider the case $H=0$; the extension to $H\neq 0$ is straightforward.

The (differential) map (17) is integrable and its phase portraits (Figs. 11 and 12) are simple: Either fixed points have smooth elliptical orbits encircling them or they have nonintersecting insets and outsets; there are also smooth, open trajectories that do not pass through or go around any fixed point. The discrete map (14) is a nonintegrable perturbation of the differential map (17); this nonintegrable perturbation is small when Eqs. (14) and (17) agree approximately, i.e., when $\xi >> 1$ (see Sec. II). When the nonintegrable perturbation is small, the Kolmogorov-Arnol'd-Moser (KAM) theorem[5,23] tells us that the phase portraits of Eq. (14) (Figs. 13, 14, and 15) must share some of the simplicity of the phase portraits of Eq. (17). In particular, only a small subset (with finite but small measure) of the elliptic orbits in Fig. 12 are destroyed by the nonintegrable perturbation. KAM trajectories (i.e., elliptic orbits that are not destroyed, only distorted) are shown in Figs. 13 and 14. The complete phase portraits of Eq. (14) are, however, very complex. In Sec. III we have described how the insets and outsets of the hyperbolic fixed points of Eq. (14) intersect each other at an infinite number of points to yield a horseshoe. In addition, the discrete map (14) also has

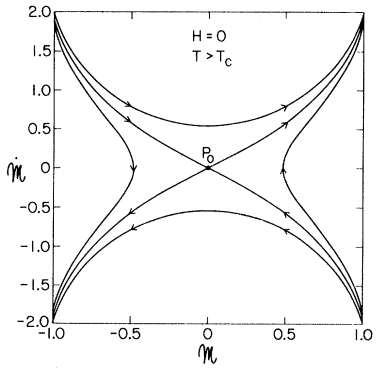

FIG. 11. Phase portrait for the continuum theory Eq. (17) in region 1 of Fig. 1. Data are the same as for Fig. 2. The fixed point P_0, its inset and outset, and some open trajectories are shown.

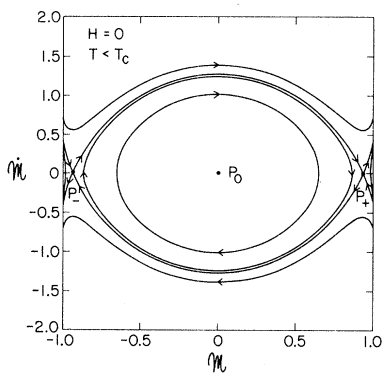

FIG. 12. Phase portrait for the continuum theory Eq. (17) in region 2 of Fig. 1, for $H=0$. Data are the same as for Fig. 4. In addition to the fixed points, P_0, P_+, and P_-, and the insets and outsets of P_+ and P_- shown in Fig. 4, the plot shows elliptic orbits that encircle P_0 and open orbits that lie outside the region bounded by the heteroclinic trajectories that connect P_+ and P_-.

periodic points or N-cycles [i.e., fixed points of $(f_1,f_2)^N$, the map (14) iterated N times] with arbitrarily large N.[39] If the fixed point of $(f_1,f_2)^N$ is elliptic, the periodic points have elliptic orbits going around them.[40] Such elliptic orbits show up clearly in Figs. 13 and 14. Nonintegrable perturbations can also yield "stochastic" or "chaotic" tra-

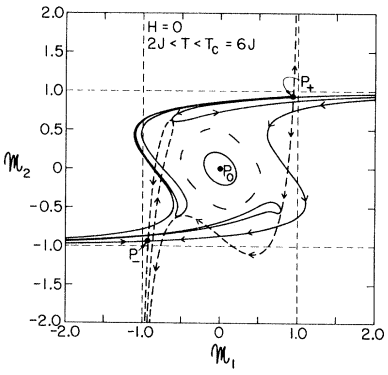

FIG. 13. Phase portrait for the discrete theory Eq. (14) in region 2a of Fig. 1, for $H=0$. Data are the same as for Fig. 12 and Fig. 5. The fixed points, P_0, P_+, and P_-, and the parts of the inset of P_- and the outset of P_+ are the same as for Fig. 5. In addition, a KAM trajectory (the "elliptic" orbit around P_0) and the seven "elliptic" orbits that go around an elliptic seven-cycle are shown. On the scale of this figure, the seven elliptic orbits show up as seven lines that lie roughly on an ellipse which encircles P_0.

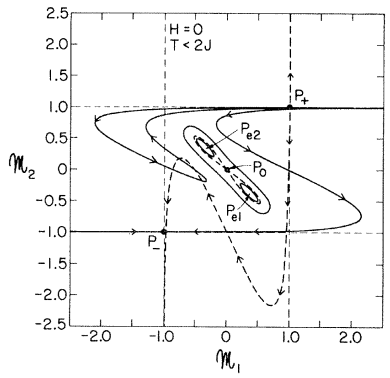

FIG. 14. Phase portrait for the discrete theory Eq. (14) in region 2b of Fig. 1, for $H=0$. Data for this plot are $d=3$, $T=1.9J$. The fixed points, P_0, P_+, and P_-, and parts of the inset of P_- (solid line) and the outset of P_+ (dashed line) are shown. The corresponding parts of the outset of P_- and the inset of P_+ may be obtained by symmetry (see text). A KAM trajectory that goes around P_0 and two "elliptic" orbits that go around the elliptic two-cycle points, P_{e1} and P_{e2}, are also shown. The broken orbit that looks like the figure eight and seems to pass through P_0 is a chaotic orbit (see Fig. 15).

jectories.[41] For the map (14), such chaotic trajectories do not lie on a one-dimensional curve but fill a two-dimensional region (see Figs. 14 and 15). The last major difference between the phase portraits of (17) and (14) is that the open trajectories for Eq. (17) have no counterparts in the phase portraits for Eq. (14); all points that lie outside the region bounded by the insets and outsets of P_+ and P_- (see Sec. III and Fig. 5) are mapped, after a finite number of iterations of Eq. (14), outside $|\mathcal{M}_i| \leq 1$, where Eq. (14) is no longer defined.

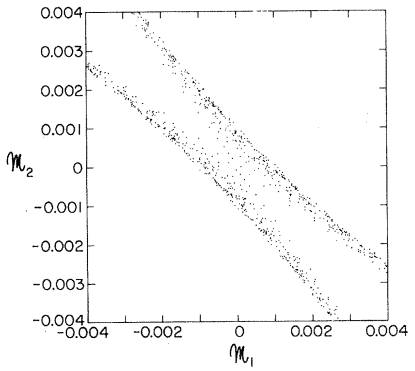

FIG. 15. Detail near P_0 of the chaotic orbit shown in Fig. 14. All the points shown in the plot were obtained using just one initial condition for the discrete map (14). Note how the chaotic orbit fills a two-dimensional region.

To make the discussion given above precise, we now describe some phase portraits of Eqs. (17) and (14) systematically (only for $H=0$). Figure 11 shows the phase portrait of Eq. (17) in region 1 of Fig. 1. There is only one fixed point, P_0, and it is hyperbolic. The insets and outsets of P_0 and selected open trajectories are shown. There are no elliptic or homoclinic orbits. The analogous phase portrait for Eq. (14) has been shown already in Fig. 3. As discussed above, it does not have any open trajectories.

Along the boundary separating region 1 and region 2(a) in Fig. 1, the fixed point P_0 is parabolic [$\sigma_1=\sigma_2=0$ for (17); $\Lambda_1=\Lambda_2=1$ for Eq. (14)]. Infinitesimally below this boundary the parabolic fixed point bifurcates into an elliptic fixed point, P_0, that remains at the origin (for $H=0$), and two hyperbolic fixed points, P_+ and P_-. Figure 12 shows the phase portrait of Eq. (17) in region 2(a) of Fig. 1. Two heteroclinic trajectories connect P_+ and P_-. Inside the region bounded by these heteroclinic trajectories there are elliptic orbits which go around P_0. Then there are the open orbits. Figure 13 shows the analog of Fig. 12 for the map (14). There is an elliptic fixed point, P_0, at the origin and two hyperbolic fixed points, P_+ and P_-. Inside the region bounded by the complicated insets and outsets of P_+ and P_- (see Sec. III B and Fig. 5) there are KAM trajectories and N cycles. The open orbits in Fig. 12 have no counterparts in Fig. 15.

For the map (17), the fixed point, P_0, is elliptic in both regions 2a and 2b of Fig. 1. However, for the map (14), at the boundary separating regions 2a and 2b in Fig. 1, P_0 becomes parabolic with reflection ($\Lambda_1=\Lambda_2=-1$). Infinitesimally below this boundary, the fixed point at the origin bifurcates into a fixed point P_0 that is hyperbolic with reflection and a pair of points, P_{e1} and P_{e2}, that constitute an elliptic 2-cycle. The inset and the outset of P_0 intersect each other at an infinite number of homoclinic points; they do not, however, intersect the insets and outsets of P_+ and P_-. Figure 14 shows the phase portrait of Eq. (14) when P_0 has become hyperbolic with reflection. We do not show the inset and outset of P_0. Instead, we show the chaotic orbit that is obtained by starting with a point near P_0 but not on its inset or outset. Figure 15 shows a magnified picture of the chaotic orbit

near P_0. Elliptic orbits that go around the 2-cycle points, P_{e1} and P_{e2}, show up clearly in Fig. 14. KAM orbits that encircle P_0 still exist and are shown in Fig. 14. All these orbits are contained in the region bounded by the insets and outsets of P_+ and P_-. There are no open trajectories.

In region 2a of Fig. 1 the elliptic fixed point P_0 undergoes an infinite number (denumerable) of bifurcations. P_0 itself remains an elliptic fixed point, while a pair of N-cycles, one elliptic and the other hyperbolic, are ejected from it.[42] Precisely at the bifurcation point, there is a parabolic N-cycle at P_0. P_0 acts as a center for the generation of pairs of N-cycles only as long as it is elliptic. The moment P_0 becomes hyperbolic with reflection, it stops bifurcating.

The N-cycles that are ejected from P_0 behave as P_0 does, if we consider the map $(f_1,f_2)^N$. If the fixed points of $(f_1,f_2)^N$ are hyperbolic (with or without reflection) they do not generate any periodic points; however, if the fixed points of $(f_1,f_2)^N$ are elliptic, they act as the centers for the generation of M-cycles of $(f_1,f_2)^N$. This sort of bifurcation ceases the moment the elliptic fixed points of $(f_1,f_2)^N$ become hyperbolic with reflection.[43]

We have already noted that Eq. (14) is a nonintegrable perturbation of Eq. (17) which is small when $\xi >> 1$, i.e., when $T \sim T_c = 2dJ$. The perturbation becomes larger and larger as $T \to 0$, and the insets and outsets of P_+ and P_- become more and more "stringy" (see Sec. III B). The area contained within the insets and outsets of P_+ and P_- becomes smaller and smaller until, at $T=0$, only nine points (all the pairs that can be formed with 1, 0, and -1, remain inside the square $|\mathcal{M}_i| \leq 1$; all other points are mapped into the region $|\mathcal{M}_i| > 1$ where the map (14) is not defined.

For the physical problems that we have considered in this paper, the only interesting parts of the phase portraits of the maps (14) and (17) have been the fixed points and their insets and outsets. It is quite conceivable that N-cycles and KAM and chaotic trajectories might be physically relevant in other physical situations. Indeed, N-cycles and KAM trajectories have been interpreted as commensurate and incommensurate phases, respectively, in systems with competing ferromagnetic and antiferromagnetic interactions.[12,44] Whether there are thermodynamically relevant chaotic trajectories is, however, a controversial question.[12,44]

---

[1] W. Selke and M. E. Fisher, Phys. Rev. B 20, 257 (1979); W. Selke and M. E. Fisher, Z. Phys. B 40, 71 (1980). These articles contain earlier references.

[2] S. A. Safran, Phys. Rev. Lett. 44, 937 (1980), and references cited therein.

[3] P. Bak, in *Solitons and Condensed Matter Physics*, edited by A. R. Bishop and T. Schneider (Springer, New York, 1978), p. 216.

[4] A three-dimensional sample has a two-dimensional surface or interface. Two-dimensional systems exhibit strong fluctuations. Fluctuation-dominated phenomena associated with roughening are, for example, missed by mean-field theory.

[5] V. I. Arnold and A. Avez, *Ergodic Problems of Classical Mechanics* (Benjamin, New York, 1968); J. Guckenheimer, J. Moser and S. E. Newhouse, *Dynamical Systems, Progress in Mathematics 8*, edited by J. Coates and S. Helgason (Birkhäuser, Boston, 1980). Also see Ref. 23.

[6] A mathematical definition of integrability may be found in Ref. 5. Roughly speaking, a dynamical system is completely integrable if there are as many independent, analytic, single-valued first integrals (constants of the motion) as there are degrees of freedom.

[7] Generalization to other lattices is straightforward.

[8] M. J. de Oliveira and R. B. Griffiths, Surf. Sci. 71, 687 (1978).

[9] J. von Boehm and P. Bak, Phys. Rev. Lett. 42, 122 (1979); J. von Boehm and P. Bak, Phys. Rev. B 21, 5297 (1980). The transitions discussed by these authors are not surface phase transitions like the layer transitions described in Ref. 8; rather, they are transitions from one bulk phase with a given modulation (of the order parameter) to another bulk phase with a different modulation.

[10] This form of the variational function $\mathcal{F}$ may be obtained by using the methods described in, H. Falk, Am. J. Phys. 38, 858 (1970).

[11] We consider a lattice which is periodically connected in the transverse directions.

[12] P. Bak, Phys. Rev. Lett. 46, 791 (1981). See also C. S. O. Yokoi *et al.*, Phys. Rev. B 24, 407 (1981).

[13] When $\xi \approx 1$, Eq. (16) can never "approximate" the spatial variation of Eq. (13). Even when $\xi >> 1$, there are solutions of Eq. (13) which have strong spatial variation and cannot be approximated by Eq. (16). It is important to know whether or not the *physical* solutions are slowly varying.

[14] The parallel is closest if one introduces the difference variable $\mathcal{M}_n \equiv \mathcal{M}_n - \mathcal{M}_{n-1}$ in the discrete case. Equa-

tion (14) then takes the form [cf. Eq. (17)]: $\mathscr{M}_{n+1} = \mathscr{M}_n + \mathscr{M}_{n+1}(\mathscr{M}_n, \mathscr{M}_n)$ and $\mathscr{M}_{n+1} = \mathscr{M}_n + (T/J)\tanh^{-1}\mathscr{M}_n - 2d\mathscr{M}_n - (H/J)$, which is area-preserving. Equation (14), which contains only the layer magnetizations themselves, is physically a little more direct than the $\mathscr{M}_n, \mathscr{M}_n$ equations above, and we shall continue to use it in the text.

[15]K. Binder and P. C. Hohenberg, Phys. Rev. B 6, 3461 (1972); 9, 2194 (1974). These articles contain extensive earlier references.

[16]The corresponding mean-field theory for the continuum fluid was given by J. W. Cahn, J. Chem. Phys. 66, 3667 (1977). The magnetic continuum case was treated in Ref. 15. The latter paper keeps terms in Eq. (15) only through $O(\mathscr{M}^4)$.

[17]Cahn (Ref. 16) assumes that the interactions between the surface and the fluid are sufficiently short-ranged, so that the contribution to the free energy of a unit area of the surface is $\Phi(C_s)$, where C_s is the limiting composition of the fluid at $n=0$. In our variables, $C_s = \frac{1}{2}[1+\mathscr{M}(0)]$, and our choice of surface couplings corresponds to $\Phi(C_s) = -H_1(2C_s-1) + (J/2)[1-2(d-1)D](2C_s-1)^2$.

[18]All figures have been constructed with $d=3$ (simple cubic lattice). Of course, Eq. (26) depends only on the combination $2dJ$; however, the inhomogeneous equations (14) and (17) and their boundary conditions are explicitly d dependent.

[19]At $T=T_c$, $H=0$, the fixed point P_0 is parabolic ($\sigma_i=0$, $\Lambda_i=1$).

[20]Aubry has studied maps similar to Eq. (14) in the context of structural phase transitions. This work is described by S. Aubry, in *Solitons and Condensed Matter Physics,* edited by A. R. Bishop and T. Schneider (Springer, New York, 1978), p. 264; S. Aubry (unpublished).

[21]The insets and outsets of the hyperbolic fixed points shown in Figs. 3, 5, and 7 were mapped out by making use of the following property: Let P be a hyperbolic fixed point of a map $\mathscr{T}$. Any line that passes through P (except its inset) is mapped, after an infinite number of iterations of $\mathscr{T}$, onto the outset of P. In practice, after only a few iterations of $\mathscr{T}$, the image of the original line is so near the outset of P that subsequent images hardly differ from one another. The inset of P may be obtained in a similar way by iterations of $\mathscr{T}^{-1}$ (of course this is possible only when the map is invertible).

[22]Figure 5 shows the form of the insets and outsets in region 2a (Fig. 1), where P_0 is elliptic. In region 2b (Fig. 1), where P_0 is hyperbolic with reflection, its insets and outsets develop homoclinic intersections and horseshoes; however, this complicated structure will not be relevant for us, since P_0 is thermodynamically unstable throughout region 2 (Fig. 1). Also see the Appendix.

[23]J. Moser, *Stable and Random Motions in Dynamical Systems,* Annals of Mathematics Studies No. 77 (Princeton University Press, Princeton, 1973); S. Smale, Bull. Amer. Math. Soc. 73, 747 (1967). See also Ref. 5.

[24]This visualization shows, for example, that the inset of P_- (P_+) will intersect the outset of P_- (P_+) at an infinite sequence of homoclinic points.

[25]Note that there are no homoclinic orbits and that kink-antikink excitations and other more complicated structures like kink-antikink-kink are not solutions of the continuum mean-field equations.

[26]Note (cf. Ref. 24) that in the discrete case there exist solutions of the mean-field equations with kink-antikink, kink-antikink-kink, etc., excitations.

[27]The surface ferromagnetic transition was first discussed by D. L. Mills, Phys. Rev. B 3, 3887 (1971). Reference 15 cites subsequent work. A mean-field treatment was done more recently by T. C. Lubensky and M. H. Rubin, Phys. Rev. B 12, 3885 (1975).

[28]Renormalization-group treatments of the surface transition have been given by T. C. Lubensky and M. H. Rubin, Phys. Rev. Lett. 31, 1469 (1973); Phys. Rev. B 11, 4533 (1973); A. J. Bray and M. A. Moore, Phys. Rev. Lett. 38, 735 (1977); J. Phys. A 10, 1927 (1977); Th. Burkhardt and E. Eisenriegler, Phys. Rev. B 16, 3213 (1977); 17, 318 (1978); N. M. Švrakić, R. Pandit, and M. Wortis, *ibid.* 22, 1286 (1980), and others.

[29]In the lattice-gas picture the local particle density is $n = \frac{1}{2}(1+\mathscr{M})$, so up (down) magnetization corresponds to high (low) density. The bulk coexistence curve lies at $H=0$, so $H<0$ at $T<T_c$ corresponds to the gas phase. $h_1>0$ represents an attractive potential exerted by the substrate on the first-layer adatoms.

[30]The phenomenon of wetting (also called spreading) is well known in a variety of systems. See, for example, N. K. Adam, *The Physics and Chemistry of Surfaces,* 3rd ed. (Oxford University Press, Oxford, 1941), Chap. VI, especially pp. 214 and 215, or W. A. Zisman, *Contact Angle, Wettability, and Adhesion* (American Chemical Society, Washington, D. C., 1964).

[31]Critical wetting disappears for $D>D_c$ [Eq. (32)]. The distinction between critical wetting (without prewetting) and first-order wetting (with prewetting) does not seem to have been made by Cahn, Ref. 16. Although his boundary condition is sufficiently general to admit both possibilities (see Ref. 17), he discusses only first-order wetting. On the other hand, D. E. Sullivan, J. Chem. Phys. 74, 2604 (1981), discusses liquid-solid wetting and finds *only* critical wetting within a van der Waals model. Within the context of the continuum mean-field theory here presented, it is clear that both possibilities are realized but for different ranges of the parameter h_1.

[32]C. Ebner and W. F. Saam, Phys. Rev. Lett. 38, 1486 (1977).

[33]C. Ebner, Phys. Rev. A 22, 2776 (1980); 23, 1925 (1981).

[34]D. E. Sullivan, Phys. Rev. B 20, 3991 (1979);

B. Widom, in *Perspectives in Statistical Physics, M. S. Green Memorial Volume,* edited by H. J. Raveche (North-Holland, New York, 1981), p. 273, discusses wetting and other properties of the interfaces between fluid phases, using dynamical analogies. For recent experimental work see M. R. Moldover and J. W. Cahn, Science 207, 1073 (1980).

[35]Appropriately formulated, the variational problem must, of course, have a solution. The resolution of this apparent paradox is to write Eq. (23) in fully continuous form,

$$L^{-(d-1)}\mathcal{F}[\mathcal{M}(x)]=\int_{-\infty}^{\infty} dx\, g\left[x,\mathcal{M}(x),\frac{d\mathcal{M}}{dx}\right],$$

with

$$g=\frac{J_1(x)}{2}\left[\frac{d\mathcal{M}}{dx}\right]^2-dJ_2(x)\mathcal{M}^2(x)$$

$$-H(x)\mathcal{M}(x)+\int_0^{\mathcal{M}(x)} dy\,\tanh^{-1}y\ ,$$

and

$$J_1(x)=J\Theta_s(x)\ ,$$

$$2dJ_2(x)=2dJ\Theta_s(x)-J[1-2(d-1)D]\delta_s(x)\ ,$$

$$H(x)=H\Theta_s(x)+h_1\delta_s(x)\ ,$$

where δ_s and Θ_s are *smoothed* versions of the usual (step) Θ function and δ function. Variation gives in place of Eq. (16)

$$\frac{d}{dx}\left[J_1(x)\frac{d\mathcal{M}}{dx}\right]+2dJ_2(x)\mathcal{M}(x)$$

$$+H(x)=T\tanh^{-1}\mathcal{M}(x)\ .$$

Integration of this equation, $\int_{-\epsilon}^{+\epsilon} dx$, across $x=0$, gives the boundary condition Eq. (24), *provided* everything varies slowly on the scale of the smoothing. Because of the $\tanh^{-1}\mathcal{M}(x)$, this proviso fails for $|\mathcal{M}(x)|\approx 1$. Thus, solutions of the smoothed problem exist in the shaded regions of Fig. 9 but depend in detail on the shapes of the smoothing functions. Note that it is quite possible that the minimum-free-energy solution of the smoothed theory develops singular behavior (e.g., a discontinuity) as the smoothing parameter goes to zero. In this situation the minimum-free-energy *continuous* solution of Eq. (16) subject to the boundary condition (36a) would not be the *physically* preferred solution. Although we have not explored the point in detail, we believe that this may well occur in and to the left of the shaded regions of Figs. 9(c) and 9(d). If so, it would eliminate the peculiar "elbow" in the prewetting line (which in this context would represent a crossover between two high-free-energy solutions).

[36]Both Refs. 8 and 33 use, in addition to h_1, a sequence of layer fields h_n which decrease with n as n^{-3}. In the strong-substrate regime, this has the effect of separating the $T=0$ layer transitions [cf. Fig. 10(b)].

[37]M. Wortis, R. Pandit, and M. Schick, in *Melting, Localization, and Chaos,* edited by R. K. Kalia and P. Vashishta (North-Holland, New York, 1982); R. Pandit, M. Schick, and M. Wortis (unpublished).

[38]It is known, for example, (see Refs. 8 and 33) that the critical points in Fig. 10(b) approach the roughening temperature rather than T_c.

[39]Indeed, when the nonintegrable perturbation [of Eq. (17)] is small and if the fixed point at the origin, P_0, is elliptic, the Poincaré-Birkhoff theorem (see Refs. 5 or 41) guarantees the existence of an infinite number of elliptic and hyperbolic N-cycles with arbitrarily large N.

[40]The elliptic orbits do not really go around the elliptic N-cycle points. A point on one of the elliptic orbits jumps (under repeated iterations of the map) from one elliptic orbit to another, until all the N elliptic orbits that encircle the N-cycle points are traced out.

[41]R. H. G. Helleman, in *Fundamental Problems in Statistical Mechanics V,* edited by E. G. D. Cohen (North-Holland, New York, 1980), p. 165.

[42]A pair of N-cycles are ejected from P_0 for $T/J=2(d-1)+2\cos(2\pi n/N)$, $n=1,2,3,\ldots$, when $H=0$. If $H=0$ and we are interested in N-cycles near the origin (i.e., P_0), Eq. (13) can be linearized (in $\mathcal{M}_n$) to give the infinite set of equations, $\mathcal{M}_{n+1}+2(d-1)\mathcal{M}_n+\mathcal{M}_{n-1}=(T/J)\mathcal{M}_n$. For an N-cycle, $\mathcal{M}_{n+N}=\mathcal{M}_n$, and the infinite set of equations becomes a set of N equations. The eigenvalues of the tridiagonal matrix on the left-hand side of the above system of equations give the "critical" values of T/J at which an N-cycle is ejected from P_0.

[43]Aubry finds similar behavior in related maps. See Ref. 20.

[44]E. Fradkin, O. Hernandez, B. Huberman, and R. Pandit (unpublished).